# Accepted Manuscript

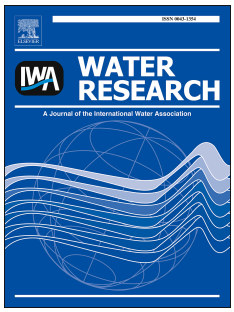


Degradation of emerging organic pollutants in wastewater effluents by electrochemical photocatalysis on nanostructured $TiO_2$ meshes

S. Murgolo, S. Franz, H. Arab, M. Bestetti, E. Falletta, G. Mascolo

PII: S0043-1354(19)30694-3

DOI: https://doi.org/10.1016/j.watres.2019.114920

Article Number: 114920

Reference: WR 114920

To appear in: *Water Research*

Received Date: 13 March 2019

Revised Date: 10 July 2019

Accepted Date: 26 July 2019

Please cite this article as: Murgolo, S., Franz, S., Arab, H., Bestetti, M., Falletta, E., Mascolo, G., Degradation of emerging organic pollutants in wastewater effluents by electrochemical photocatalysis on nanostructured $TiO_2$ meshes, *Water Research* (2019), doi: https://doi.org/10.1016/j.watres.2019.114920.

# Degradation of Emerging Organic Pollutants in Wastewater Effluents by Electrochemical Photocatalysis on Nanostructured $TiO_2$ Meshes

S. Murgolo[1], S. Franz[2], H. Arab[2], M. Bestetti[2], E. Falletta[3], G. Mascolo[1]*

(1) CNR, Istituto di Ricerca Sulle Acque, Via F. De Blasio 5, 70132 Bari, Italy

(2) Politecnico di Milano, Department of Chemistry, Materials and Chemical Engineering, „G.Natta“, Milano, Italy

(3) Università di Milano, Dipartimento di Chimica, Milano (Italy)

* Corresponding author. Tel.: +39 080 5820519; fax: +39 080 5313365.

*E-mail address:* giuseppe.mascolo@ba.irsa.cnr.it (G. Mascolo).

**Abstract**

An immobilized photoactive $TiO_2$ coating grown directly on titanium meshes was successfully exploited for the electrochemical photocatalytic degradation of carbamazepine in real secondary wastewater effluent. The catalyst was prepared by Plasma Electrolytic Oxidation and during the photocatalytic water treatment an electrical polarization (bias) was applied to the catalyst. The investigated process was compared with the conventional one employing suspended $TiO_2$ powder (Degussa P25). Results showed that carbamazepine degradation rate follows the order UV/supported $TiO_2$+bias ≈ UV/$TiO_2$ Degussa P25 > UV/supported $TiO_2$ > UV. The investigation also included the identification of other micropollutants and degradation products. This allowed the detection of 201 compounds present in the secondary wastewater effluent employed for the photocatalysis tests, 51 of them also successfully associated to compounds of emerging concern (CECs), and 194 to transformation products (TPs). The degradation of detected compounds followed first-order kinetics and the mean kinetic constant values of the 51 CECs resulted to be 0.048, 0.035 and 0.043 $min^{-1}$ for the $TiO_2$+Bias+UV, $TiO_2$+UV and UV, respectively. As for TPs, results showed that the $TiO_2$+Bias+UV treatment is much more efficient than both $TiO_2$+UV and UV in minimizing the intensity of the organics in the real wastewater. Such a better performance was more pronounced at higher reaction time reaching 60 % reduction of mean peak area of TPs at 90 min of reaction. Among the detected TPs also compounds belonging to known carbamazepine TPs were found. This allowed to propose a degradation pathway of carbamazepine. The supported catalyst was positively tested for 15 cycles demonstrating that it has the potential to be used in real wastewater tertiary steps aimed at removing CECs.

**Keywords:** immobilized catalyst; titanium dioxide; compounds of emerging concern; secondary wastewater effluent; non-target screening; transformation products.

## 1. Introduction

Water resources and societal wellbeing are currently threatened by contaminants of emerging concern (CECs) as well as by pathogens including antibiotic resistant bacteria and viruses. The impact of wastewater effluents containing CECs on the quality of receiving water bodies has been widely demonstrated (Kasprzyk-Hordern et al. 2009, Zhou et al. 2009). Removal of CECs and/or their metabolites is related to both the nature of the specific organics and to the treatment methods employed in the treatment plant (Castiglioni et al. 2018, Joss et al. 2005, Loos et al. 2013). CECs can be also degraded into products that are still active (Rizzo et al. 2019, Stalter et al. 2010, Ternes 1998, Zwiener et al. 2002).

Wastewater reuse has been prompted as a new challenge due to the ever increasing demand of fresh water caused by the growth of population and the high consumption in agricultural and industrial sectors. Water recycling for non-potable uses from conventional water treatment processes is applied in water-scarce regions and it can be among the driving forces for the requirement of water of better quality. The relevance of addressing the issue of CECs was acknowledged by the Directive 2013/39/EU listing priority substances and further supported by the implementation of Decision (EU) 2015/495 on March 20, 2015 establishing a watch list

including 10 target substances for European Union-wide monitoring (Schröder et al. 2016, Sousa et al. 2018). The watch list was recently revised by the Decision (EU) 2018/840. It follows that requirement of water of better quality acts as a driving force for the application of post-treatment technologies in wastewater treatment plants (WWTPs). Conventional wastewater treatment processes lead to incomplete removal of CECs (Luo et al. 2014, Tran et al. 2018) being not designed to perform such organics removal. Advanced biological treatments showed better performance than conventional ones for selected CECs removal (Balest et al. 2008). It is worth noting that, due to the driving force of preserving the environmental quality of receiving water bodies, the environmental legislation of countries such as Switzerland was modified in order to achieve 80% removal of among 6 CECs from a list of 12 compounds (Giannakis et al. 2015, Logar et al. 2014). Advanced oxidation processes (AOPs), including photocatalysis, can remove a large range of organic micropollutants and CECs (Fagan et al. 2016, Miklos et al. 2018, Pagano et al. 2008), being also possible their integration with biological processes (Del Moro et al. 2013, Del Moro et al. 2016). Heterogeneous photocatalysis has become relevant in the last years since sometimes chemicals are not necessary for the oxidation processes (Andronic et al. 2016, Cates 2017, Dong et al. 2015). For example, the use of titanium dioxide ($TiO_2$) as a photocatalyst is receiving growing attention for its effectiveness, due to the nonspecific nature of the reactive species produced under UV irradiation (Nakata and Fujishima 2012, Ochiai and Fujishima 2012). However, it has to be considered that the efficiency of the process still needs to be improved due to both the low quantum efficiency of the process, namely too many photons are not used to produce hydroxyl radicals, and possible catalyst poisoning especially with real wastewater. In addition, the application of suspended $TiO_2$ is very limited at both pilot

and full-scale since the small size of the catalyst complicates its recovery at the end of the treatment, reducing its potential reuse and compromising the quality of treated effluent (Byrne et al. 2017). To overcome this drawback, several authors have studied the immobilization of $TiO_2$ particles on different materials (Borges et al. 2015, Comparelli et al. 2004, Murgolo et al. 2017, Petronella et al. 2013, Petronella et al. 2011). However, despite the huge number of papers available in the literature, real applications of photocatalysis with supported catalysts are still very rare.

Electrochemical $TiO_2$ photocatalysis is a well-known technique among AOPs for water treatment but a not often applied process. The photoactive coating is grown directly on the titanium meshes, leading to good mechanical adhesion to the substrate and good electrical conductivity. During the wastewater treatment step aimed at removing organic pollutants, an electrical bias can be effectively applied to the catalyst through the mesh, leading to a synergistic effect with UV light and a faster degradation kinetics with respect to either photocatalytic or the electrochemical process.

Photoactive $TiO_2$ coatings are obtained by a number of techniques including sol-gel, CVD, RF magnetron sputtering, plasma spray, electron beam evaporation, anodic oxidation (AO) (Bestetti et al. 2007) and plasma electrolytic oxidation (PEO) (Franz et al. 2016). Catalysts obtained by PEO and AO were already proved to be effective in the degradation of a model dye (Franz et al. 2015). The experimental set-up for PEO and AO are similar. However, due to the high operating voltage applied during PEO, very peculiar physico-chemical conditions are established (Yerokhin et al. 1999), promoting high growth rates (roughly 1 μm/min), oxide crystallization and incorporation of chemical species from the electrolyte (Bayati et al. 2010,

Franz et al. 2016, Mirelman et al. 2012). Due to these features, since the '70s the PEO process has found industrial applications to obtain oxide protective layers on aluminum and magnesium (Yerokhin et al. 1999), and titanium alloys, mostly Ti-6Al-4V for biomedical implants (Liu et al. 2005, Nie et al. 2000, Wei et al. 2008).

In the present study, the effectiveness of the electrochemical photocatalysis employing immobilized $TiO_2$ obtained by PEO was tested for the removal of CECs by treating a real secondary wastewater. The wastewater was also spiked with carbamazepine, which is one of the main CECs in municipal wastewaters. In order to get insights about the degradation pathway in the real water matrix, an identification of the transformation products (TPs) formed during the photocatalytic treatment of secondary wastewater effluent was performed, too. Finally, the supported catalyst was positively tested for 15 cycles demonstrating that it has the potential to be used in real wastewater tertiary step aimed at removing CECs.

## 2. Materials and methods

### 2.1. Preparation of nanostructured $TiO_2$ Meshes

Titanium dioxide coatings were obtained by PEO of grade I titanium expanded meshes in 1.5 M $H_2SO_4$ (14.7 wt. %), at constant potential of 150 V, for 5 mins. Several smaller samples (18 $cm^2$ area) were also produced in the same conditions for further characterization. Visually, all the samples had a light gray and uniform appearance. The electrolyte temperature was set at about -5 °C by a cryostat (HAAK D10). After PEO, the samples were rinsed with water and dried in a stream of air.

Morphology was investigated by scanning electron microscopy (SEM) using a Zeiss EVO 50 instrument. The phase structure and texture of the titanium dioxide films were assessed by X-ray diffraction (XRD) using a Philips PW1830 instrument operating in Bragg-Brentano geometry at a potential of 40 kV with a filament current of 40 mA. Diffractograms were acquired with Cu $K_{\alpha 1}$ radiation in the 2θ range 20–60° at the scanning rate of 2.5° per min. The XRD patterns were indexed according to the powder diffraction files of titanium (ICDD-PDF 44-1294), anatase (ICDD-PDF 21-1272) and rutile phases (ICDD-PDF 21-1276). The mass fraction of anatase was calculated according to Eq. 1 (Spurr and Myers 1957), where $I_R$ is the intensity of the strongest rutile reflection, (110), and IA is the intensity of the strongest anatase reflection, (101),

$$f_A = \frac{1}{\left(1+1.26\frac{(I_R)}{(I_A)}\right)}\% \qquad \text{Eq. 1}$$

Surface porosity was evaluated by analyzing several SEM surface micrographs taken at 20,000x magnification using ImageJ analysis software. Film thickness and depth profiling were assessed by Glow Discharge Optical Emission Spectrometry (GD-OES) using a Spectruma GDA750 analyzer operated at 700 V in argon atmosphere at 230 Pa. The area of analysis was of ~2.5 mm diameter, and the monitored light emissions during the analysis were 130 nm and 362 nm for oxygen and titanium, respectively. The photocurrent density of the $TiO_2$ film was measured by Linear Sweep Photo-Voltammetry (LSPhV) in 4.2 mM KCl aqueous solution with and without irradiation at a scan rate of 5 mV $s^{-1}$ and room temperature using a potentiostat/galvanostat (Solartron Analytical ModuLab ECS). The reference electrode was a Saturated Calomel Electrode (SCE). The counter electrode was a Ti-6Al-4V mesh. The exposed area during LSV was 4 $cm^2$. The photocurrent measurements were repeated three times. The Incident Photon-to-Current Efficiency (IPCE) was calculated using the equation 2

$$IPCE(\%) = \frac{h*c}{e} * \frac{I}{P*\lambda} \qquad \text{Eq. 2}$$

where h is the Plank constant [$m^2 Kg\ s^{-1}$], c is the speed of light [$m\ s^{-1}$], e is the electron charge [C], I is the steady-state photocurrent density [$A\ m^{-2}$], P is the light intensity [$W\ m^{-2}$] and λ is the incident wavelength. The IPCE values were taken under polarization at 1.5 V vs SCE. The electrochemical surface area (ECSA) of the $TiO_2$ obtained by PEO was estimated by cyclic voltammetry (Trasatti and Petrii 1991), where consecutive potential cycles centered around the open potential circuit were recorded in a potential range -0.52 ÷ -0.42 V *vs.* SCE at five different scan rates.

## 2.2. Organic pollutants and wastewater characteristics

Wastewater was collected at the outlet of the aerobic biological step (suspended biomass) from a WWTP of the area of Milan, Italy, that includes grit and grease removal step, biological oxidation-nitrification sections, denitrification, secondary sedimentation steps, disinfection. The physicochemical parameters were determined according to Standard Methods (Rice et al. 2012) and are listed in Table 1 together with the relevant figures of the selected WWTP. Wastewater samples were first filtered on paper filter to remove coarse materials and then on 0.2 µm glass filter. Filtered wastewater was spiked with carbamazepine (Sigma-Aldrich) at concentration of 100 µg $L^{-1}$ before running the photocatalytic experiments. The spiking concentration was chosen in order to obtain a good compromise between having a concentration high enough to be able to detect a number of transformation products and low enough to be close to real environmental conditions.

178 **2.3. Experimental setup**

179 The process was carried out in a laboratory-scale 1 L tubular photocatalytic reactor equipped
180 with a 1 L buffer reservoir working in semi-batch mode under electrical polarization (bias) of
181 the expanded mesh (geometric surface area 327.5 $cm^2$). The sketch of the employed reactor is
182 shown in Figure S1 (Supplementary Material). The UV source consisted of a 30 W low-pressure
183 Hg vapor lamp UV-C lamp emitting at 254 nm. Accordingly, four different configurations with
184 the explained reactor were investigated as follow: $TiO_2$+UV+bias, $TiO_2$+UV, $TiO_2$+bias, and only
185 UV. Control tests with the conventional suspended catalyst were carried out with a batch
186 reactor (1 L) equipped with a 30 W low-pressure Hg vapor lamp (Helios Italquartz). The
187 employed conventional catalyst was Degussa P25 (Evonik) $TiO_2$, consisting of anatase and rutile
188 crystallites with a ratio typically of 80:20, a surface area of 50 $m^2\ g^{-1}$ and an average diameter of
189 30 nm. The radiance density flux at 254 nm was measured through actinometry test using 10
190 μM uridine (Sigma-Aldrich).

191

192 **2.4. Chemical analysis**

193 The monitoring at various reaction times of the residual concentration of spiked
194 carbamazepine, of the other compounds detected in the employed wastewater and the
195 investigation of TPs (see next section) was carried out by an Ultimate 3000 UPLC System
196 (Thermo Fisher Scientific) equipped with an autosampler, temperature-controlled column
197 compartment and UV detector as a chromatographic system that was interfaced with a high-
198 resolution mass spectrometer, TripleTOF® 5600+ System (AB Sciex) equipped with a duo-spray
199 ion source that was operated in electrospray (ESI) mode in positive and negative ion modes. MS

200 analysis was carried out by an information dependent analysis (IDA) method that includes a
201 survey scan in TOF-MS and, after background subtraction, the isolation and fragmentation in
202 the collision cell of the four most intense ions.
203 The chromatographic separation of the organic mixtures was performed by injecting 500 µL
204 samples, according to the so-called large volume injection mode, and eluting them at 0.200 mL
205 $min^{-1}$ through a BEH C18 column, 2.1 x 150 mm, 1.7 µm, with a binary gradient consisting of
206 $H_2O$/ACN 95/5, 0.1% HCOOH (A) and ACN, 0.1% HCOOH (B). The large volume injection mode
207 was used in order to reach limit of detection of the order of few ng $L^{-1}$, namely the
208 concentration of CECs usually found in real wastewater effluents. The gradient started from 5 %
209 B that was held for 4.6 min and then was linearly increased to 80 % in 18.5 min and to 100 % in
210 further 5.5 min and the final composition was held for 0.5 min. At the end of each run, the
211 system was further rinsed for 6 min using the final eluent composition and then returned to
212 starting conditions and equilibrated for 5 min. The residual concentration of carbamazepine
213 was obtained by MultiQuan 3.0.2 software (AB Sciex).
214

215 **2.5. Suspects screening, non-target screening and transformation products identification**
216 While targeted LC–tandem MS (liquid chromatography–mass spectrometry) methods are
217 specifically designed to analyze and quantify a set of previously defined target compounds,
218 non-target approaches make use of modern high speed and high resolution mass
219 spectrometers (HRMS) to gather as much information as possible about any detectable
220 substance. All the collected IDA-MS data files, corresponding to the different reaction times for
221 a specific treatment, were processed for non-target screening using a data workflow in

enviMass 3.4 software (Loos 2018). Briefly, the approach used for the interpretation and processing of data is as follows: an initial enviMass peak picking step generates a list of ions with a corresponding retention time and peak intensity in each acquired file. The list of ions was subsequently reduced by replicate sample intersection, removal of peaks which have also been detected in blank samples, isotope grouping and adduct grouping. The obtained peak lists were then processed by SciexOS software for detecting significant trends as well as for identification of unknown compound, employing both the formula finder based on isotopic pattern and library searching capabilities (LibraryView). Structure identification was then attempted based on high resolution MS-MS data (Detomaso et al. 2005). Moreover, linking these results to ChemSpider and Metlin, a more confident identification of detected compounds in investigated samples was performed (Guijas et al. 2018). The peaks for which a typical trend of transformation products was identified were further processed by R statistical environment, using a linkage analysis script, in order to obtain further information about the occurrence of possible TPs (Schollée et al. 2018).

## 3. Results and discussion

### 3.1. Characterization of nanostructured $TiO_2$ meshes

As shown by the SEM micrograph of the surface of the $TiO_2$ coating in Figure 1a, the oxide layer is porous with an interconnected sponge like morphology. The average surface porosity obtained by analyzing the SEM surface micrograph is about 10 %. However, the cross-section SEM micrograph (inset of Figure 1a) revealed that the coatings are increasingly compact in

depth. The GDOES depth profiles of the titanium and oxygen elements shown in Figure 1b confirmed that the thickness of the $TiO_2$ coating is roughly 2.5 µm. According to the XRD patterns shown in Figure 1c, the as-prepared $TiO_2$ films are crystalline in structure. The mass fraction of the anatase and rutile phases calculated following Spurr (Spurr and Myers 1957) are 58 % and 42 %, respectively. Based on the UV-visible spectra and the corresponding Kubelka-Munk conversion using the Tauc-plot method (Figure S2) a band gap of 3.06 eV was calculated, as expected considering the band gap of pure anatase (3.2 eV) and pure rutile (3.02 eV).

The photoelectrochemical activity of $TiO_2$ coating was assessed by measuring the photocurrent of the films under electrical bias, i.e. by linear voltammetry in dark and under UV-C irradiation from 0 V to 1.5 V (*vs.* SCE). The photocurrent density initially increases steeply with the potential, and then it stabilizes on a well-developed plateau at 0.174 mA $cm^{-2}$ and 0.96 V *vs.* SCE. The corresponding IPCE, which is defined as the number of electrons generated by light in the external circuit divided by the number of incident photons, more clearly represents the photoelectrochemical activity of the coatings. In agreement with the photocurrent density, the IPCE initially linearly increases with the applied voltage and then it stabilizes at a maximum value of 65%.

The previous characterizations were carried out on sacrificial samples obtained in the same experimental conditions as for the expanded mesh employed in the reactor. From the practical point of view, linear sweep photovoltammetric measurements carried out in situ by keeping the mesh in the reactor. This allows an easily monitoring of the activity of the $TiO_2$ catalyst grown on the expanded mesh. Additionally, based on the photocurrent response of the mesh, the electrochemical polarization voltage to be applied at the catalyst during operation can be

266 selected and possible phenomena of shielding of the $TiO_2$ film due to the anodic deposition of
267 dispersed particulate or oxidation by-products can be detected. In Figure S3, the resulting
268 photocurrent response from 0 V to 5 V (cell voltage) is shown. In agreement with
269 measurements carried out on sacrificial samples, the photocurrent shows an initial sharp
270 increase followed by a plateau.
271 The minimum surface area of the $TiO_2$ catalyst employed in the electrochemical photoreactor
272 corresponded to 327.5 $cm^2$, i.e. the geometrical area of the expanded mesh itself. However, the
273 real surface area is expected be higher than the geometrical area of the titanium substrate due
274 to the porous morphology. In order to estimate the real surface area involved in the
275 photoelectrochemical process, the electrochemical surface area (ECSA) of the catalyst was
276 measured (Trasatti and Petrii 1991). The ECSA was calculated on the basis of the capacitive
277 current due to the double-layer charging and discharging at the solid–electrolyte interface in
278 the non-faradaic region of the cyclic voltammograms. The resulting total intensive capacitance
279 of about 48.2 µF $cm^{-2}$ was compared to the experimental intrinsic specific capacitance, which
280 was about 0.88 µF $cm^{-2}$, leading to a real surface area of 54.8 $cm^2$ per $cm^2$ of geometrical area.
281 This corresponds to around 5.7 $m^2$ $g^{-1}$, which is a reasonable value considering that $TiO_2$
282 nanopowders have real surface area of the order of 150 $m^2$ $g^{-1}$. Therefore, the total ECSA of the
283 catalyst used in the electrochemical photoreactor was 1.795 $m^2$. Comparatively, the control
284 tests in the batch reactor were carried out using a total amount of conventional suspended
285 catalyst of 100 mg $L^{-1}$, corresponding to a real surface area of 5 $m^2$.
286

### 3.2. Photocatalytic removal of CECs

The degradation of carbamazepine, which was initially spiked at 100 μg $L^{-1}$ in the wastewater effluent, by the conventional photocatalysis with suspended Degussa P25 and by electrochemical $TiO_2$ photocatalysis is depicted in Figure 2. Results show that with the two above mentioned photocatalytic processes the carbamezapine was completely removed within 45 min. The degradation by the conventional suspended catalyst showed a slightly faster removal in the first stage of the reaction, namely between 5 and 30 min. The beneficial effect of applying a polarization potential (bias) to the supported $TiO_2$ catalyst is also evident from Figure 2 since the reaction performed without any bias showed a much slower carbamazepine degradation being about 20 % the residual carbamazepine after 90 min of reaction. Also, reaction performed with conventional and electrochemical photocatalysis shows a faster carbamazepine removal than photolytic process. A more equitable comparison could be obtained where the results of actinometry test in both conventional and electrochemical photocatalysis conditions are considered. In particular, it was revealed that in case of electrochemical photocatalysis, the presence of the mesh introduces a shielding effect of almost 66% remaining an amount of radiance density flux as 0.08 W $cm^{-2}$ while in the case of conventional photocatalysis, the shielding effect was measured as 6.74% corresponding to a flux of 0.15 W $cm^{-2}$. Overall, the results displayed in Figure 2 demonstrate the effectiveness of electrochemical photocatalysis with supported $TiO_2$ catalyst. Specifically, even though the performance of the electrochemical $TiO_2$ photocatalysis showed to be similar to the photocatalysis with the conventional suspended $TiO_2$, the former process has the advantage of avoiding using a suspended catalyst that is known to be difficult to be removed at the end of

309 the water treatment process. In addition, the supported catalyst was positively tested for 15
310 cycles showing that the performance, based on pseudo-first order kinetic constants, remained
311 in the range of 75-100 % (Figure 3a). After a prolonged use (several tenths of reactions) the
312 catalyst showed a reduced performance. However, the initial performance was recovered by a
313 chemical cleaning in dilute HCl solution or, eventually, by a re-anodization process (Figure 3b).
314 In order to get deeper insights about the effectiveness of the novel catalyst, the comparison of
315 the electrochemical photocatalysis with respect to both photocatalysis with the same
316 supported $TiO_2$ catalyst and photolysis was also performed for the CECs naturally present in the
317 secondary wastewater effluent. An analytical screening was carried out, as described in the
318 section 2.5, aimed at identify as many as possible CECs. The procedure led to the detection of
319 201 compounds present in the secondary wastewater effluent employed for the photocatalysis
320 tests and 51 of them were also successfully associated to CECs on the basis of the positive
321 match of both the isotopic cluster of molecular ion and the product ion spectrum with that of
322 the available MS library. The decay of the 51 identified CECs was found to follow first-order
323 kinetics and the distribution of their kinetic constants are shown in Figure 4a. Boxplots built
324 with all obtained kinetic constant values show the higher performance of the electrochemical
325 photocatalysis with respect to the experiment where the bias was off ($TiO_2$+UV) as well as to
326 the photolysis. Specifically, the median values of the 51 kinetic constants resulted to be 0.044,
327 0.023 and 0.034 $min^{-1}$ for the $TiO_2$+Bias+UV, $TiO_2$+UV and UV, respectively. A similar trend with
328 the highest values for the $TiO_2$+Bias+UV process was found when considering the mean kinetic
329 constant value (0.048, 0.035 and 0.043 $min^{-1}$, respectively) and the 25-75 % percentile range
330 used for building the boxplots (0.02-0.069, 0.007-0.053 and 0.009-0.059, respectively).

From the first-order kinetic constants, it can be easily obtained the half-life times of each suspect CECs. All the results were plotted as boxplots and the results showed, once again, the superior performance of the electrochemical photocatalysis (Figure 4b). Specifically, a mean half-life time of 28.1 min was calculated for the $TiO_2$+Bias+UV process with respect to 80 and 62.3 min for the $TiO_2$+UV and UV treatments, respectively. In addition, from the first-order kinetic constants the Electrical Energy per Order of magnitude of removal ($E_{EO}$), expressed in kWh $m^{-3}$, can be calculated using equation 1 (Murgolo et al. 2017):

$$= \frac{38.4 \ x \ UV \ power \ (kW)}{V \ (L) \ x \ k \ (min^{-1})} \quad (1)$$

where *k* is the first-order rate constant ($min^{-1}$) for the disappearance or the target CECs, V is the water volume to be treated and UV power is obtained from the employed UV lamp. As expected, the obtained results (Figure 4c) show the lower energy requirements of the electrochemical photocatalysis being the $E_{EO}$ values 46.8, 133 and 103.5 kWh $m^{-3}$, for the for the $TiO_2$+Bias+UV process with respect to the $TiO_2$+UV and UV treatments, respectively. Indeed, the obtained $E_{EO}$ values when translated into electrical operating costs would lead to values at least one order of magnitude higher than those calculated for CECs removal at full scale WWTPs. It has to be taken into account that the employed experimental system is a small lab-scale reactor and consequently its electrical operating cost cannot be compared with that of full-scale systems.

Overall, the above-described results demonstrate that the novel supported $TiO_2$ catalyst employed for the electrochemical photocatalysis is effective in removing not only the spiked carbamazepine at 100 µg $L^{-1}$ but, more importantly, a high number of CECs present in the real secondary wastewater effluent.

352

353 **3.3. Minimization of transformation products**

354 Beside the degradation of CECs present in the employed secondary wastewater effluent, it is
355 also important to assess the TPs arising from the treatment by electrochemical photocatalysis
356 with the novel supported $TiO_2$ catalyst with respect to both photolysis and photocatalysis with
357 the same supported catalyst. The employed analytical protocol for the screening of non-target
358 organics allowed detecting compounds not present in the secondary effluent at the beginning
359 of the UV-based experiments that could be thus confidently associated to TPs. Using the same
360 protocol, the detection of compounds initially present in the employed wastewater and
361 increasing along reaction time was also accomplished. Consequently, the latter compounds
362 were associated to TPs, too. By a careful inspection of the detected compounds as output of
363 the aforementioned analytical protocol, 194 TPs were rationally identified (Table S2). The
364 detected TPs showed to follow three different types of time profiles, namely (i) a bell-shape
365 trend, (ii) slight increase followed by a steady time-profile, (iii) a constant increase along
366 reaction time. TPs with the latter two time-profiles were thus accumulating in the reaction
367 mixture.

368 Indeed, a number of TPs were surely arising from the organic matter contained in the real
369 wastewater rather than from CECs. Therefore, considering the high number of TPs detected,
370 the comparison of the three UV-based processes was performed based on average peak
371 intensity. In Figure 5a are depicted the results of the 194 TPs for the three UV-based treatments
372 at both the final reaction time (90 min) and the middle reaction time (45 min) in comparison
373 with the initial wastewater. The boxplots of Figure 5a clearly show the higher performance of

the electrochemical photocatalysis with respect to both the experiment where the bias was off ($TiO_2$+UV) and the photolysis. Specifically, the mean peak area for $TiO_2$+Bias+UV at 45 min reaction time resulted to be almost the half those of the other two treatments (183500, 31200 and 35900 for the $TiO_2$+Bias+UV, $TiO_2$+UV and UV, respectively). Results obtained at 90 min reaction time show that such a difference between $TiO_2$+Bias+UV and the other two processes further increased being the mean peak area one-third of the other two reactions. It is worth noting that the mean peak area value obtained by $TiO_2$+Bias+UV after 90 min is only 67 % of that of the initial wastewater (110000 with respect to 163000) because only the detected 194 TPs were considered where, most of them, were not present in the initial wastewater. When both the detected 194 TPs and the 201 compounds present in the secondary wastewater effluent employed for the photocatalysis tests (51 of which were associated to CECs) were considered, different results were obtained (Figure 5b). Specifically, the mean peak area value of the initial wastewater was similar to those of the $TiO_2$+UV and UV treatments at both 45 and 90 min but the correspondent values of the $TiO_2$+Bias+UV treatment were consistently lower. In addition, Figure 5b shows that, even though several TPs were detected, after just 45 min of reaction the three investigated processes were able to lead an average peak area of all detected compounds lower than the initial value, being that of the $TiO_2$+Bias+UV treatment the lowest. This demonstrates that that the $TiO_2$+Bias+UV treatment is much more efficient than both $TiO_2$+UV and UV in minimizing the intensity of the organics in the real wastewater. Such a better performance was more pronounced at higher reaction time reaching 60 % reduction of mean peak area of TPs at 90 min of reaction.

### 3.4. Identification of transformation products and carbamazepine degradation pathway

In order to get insights about the occurrence of TPs arising from possible transformation reaction the linkage analysis was employed (Schollée et al. 2018). The linkage analysis is based on the fact that a transformation reaction is associated to an accurate mass difference between the parent compound and the TP. As the analytical screening was performed by high resolution-mass spectrometry for all detected compounds the accurate mass was obtained (Tables S1 and S2). A list of possible transformation reactions was built on the basis of reactions likely to occur during UV-based processes and each reaction is consequently associated to an accurate mass difference (Table 2). The list of parent compounds detected in the initial wastewater (table S1) was then compared with the list of detected TPs (Table S2) in order to obtain the couples of parent/TP whose accurate mass difference match one of those listed in Table 2 within the set mass tolerance. As expected, results showed that the highest number of transformations were those compatible with oxidative reactions likely to occur during photocatalysis (Figure 6). Specifically, four transformation reactions (addition of 2 atoms of oxygen, addition of 3 atoms of oxygen, hydroxylation/N or S-oxidation/epoxidation, alcohol to carboxylic acid) were found to have 8, 4, 7 and 10 couples of parent/TP that could be positively associated to them. The hydration reaction was found to be the transformation reaction with the highest number (11) of matches. This reaction occurred on compounds with carbon-carbon double bonds present in the wastewater matrix and the UV light made the hydration reaction likely to occur. It is worth noting that beside the hydration reaction also the de-hydration reaction was found to have 6 positive matches. It follows that both the hydration and de-hydration occur during UV-based processes with real wastewater due to the chemical composition of the real water matrix and

418 to the combination of UV light and temperature increase as a consequence of UV lamp energy
419 dissipation. In addition, a relevant number of positive matches were also observed for reaction
420 likely due to photolysis, namely di-demethyl or de-ethylation (9 matches), demethylation and
421 de-acetylation (6 matches for each reaction), dealkylation (5 matches).
422 The linkage analysis was also carried out using, as parent compounds, the list of 51 suspect
423 CECs identified within the 201 compounds detected in the initial wastewater. Results (Figure 6,
424 red lines) showed that the distribution of detected transformations was similar to the previous
425 linkage analysis. Specifically, the highest number of matches were obtained for the alcohol to
426 carboxylic acid reaction, de-hydration, dealkylation (4 matches for each transformation) and
427 hydroxylation/N or S-oxidation/epoxidation, hydration, dealkylation (3 matches).
428 In addition, as carbamazepine was spiked in the real wastewater at beginning of the reaction,
429 the couples of parent/TP detected by the linkage analysis were inspected in order to find those
430 that matched the known TPs of carbamazepine. Six carbamazepine TPs were positively
431 detected that allowed to drawn the degradation pathway depicted in Figure 7. It is worth
432 noting that all the TPs of Figure 6 were positively identified on the basis of accurate mass of
433 molecular ion, elemental composition using the isotopic cluster of molecular ion and MS-MS
434 spectra. Therefore, the identification level of such TPs was 2 (probable structure) according to
435 Schymanski et al. (Schymanski et al. 2014). The TP250 (Figure 7) was rationalized to derive from
436 TP268 (and not from carbamazepine by the alcohol to carboxylic acid or primary amine to nitro
437 reaction that was also detected by the linkage analysis) by a hydration reaction as this TP was
438 also detected in the initial wastewater. TP223 was found by the linkage analysis as parent of the

TP179 (acridine) and it was rationalized to derive from carbamazepine as a result of multiple transformations.

In Figure S4 the time-profiles of the TPs of Figure 6 are depicted, showing that the electrochemical $TiO_2$ photocatalysis allowed a higher minimization of their abundances with respect to both photolysis and photocatalysis with supported $TiO_2$. These results confirmed what above reported about the better performance of the investigated process. It is worth noting that the time-profiles show that at higher reaction time the TPs disappear likely forming low-molecular weight organic acids as final degradation products that are not detectable by the employed chromatographic column being necessary to use ion chromatography (Mascolo et al. 2005). It worth noting that the formation of such further TPs would not be easily detectable in the employed real effluent since carboxylic acids could exists as coming from other processes and other organic compounds.

By inspecting the couples of parent/TP detected by the linkage analysis it was also possible to find some compounds that underwent transformation reactions. These compounds are not included in the list of suspect CECs and therefore are likely to be compounds present in the water matrix of the employed real wastewater. The reactions detected by the linkage analysis were, most of the times, oxidation reactions that are consistent with the investigated processes. A typical example is related to the parent compound of accurate mass 141.1154 ($[M+H]^+$ = 142.1218) whose elemental composition was determined to be $C_8H_{15}NO$. This compound is likely to be 1-piperidinoacetone even though two other chemical structures are possible, namely tropine and azonan-2-one. For the parent compound the linkage analysis detected two oxidative transformation products as depicted in the degradation pathway of

461 Figure 8 where the chemical structure of two other possible parent compounds are shown, too.
462 The chemical structure could not be identified unequivocally due to lack of MS-MS spectra and
463 authentic standard. Overall, the linkage analysis demonstrated to be a useful tool for selecting
464 the TPs to be further investigated among the full list of TPs.
465
466
467 **4. Conclusions**
468 The application of an electrochemical photocatalytic process based on the use of an innovative
469 photoactive coating grown directly on titanium meshes was evaluated for the degradation of
470 pharmaceuticals in real secondary wastewater effluent. Carbamazepine and other CECs were
471 more rapidly phototransformed compared to only photolysis, regardless the water matrix. It
472 was demonstrated that the supported catalyst can be easily reused without losing efficiency.
473 The fate of 194 metabolites formed during the investigated treatments was assessed, observing
474 a higher performance of the electrochemical photocatalysis with respect to both the
475 experiment where the bias was off ($TiO_2$+UV) and the photolysis. Results show that non-target
476 evaluation can give additional information to assist process evaluation beyond the analysis of
477 single “target” micropollutants. The suspect search allows a wider spectrum of micropollutants
478 to be monitored (e.g., due to a decrease in treatment performance) and can be used to
479 annotate non-target peak lists to identify the peaks which are already known prior to further
480 non-target evaluation. Finally, the possible scale-up of the proposed water treatment could
481 take advantage from the fact that the catalyst is prepared by a technique already in use in the
482 industry of surface treatments. As far as information about operating costs is concerned, it can

be stated that the investigated process is less energy demanding of the other two tested processes. However, as the employed experimental reactor is a small lab-scale system, the obtained $E_{EO}$ values when translated into electrical operating costs would lead to values at least one order of magnitude higher than those calculated for CECs removal at full scale WWTPs. It follows that the new investigated process still needs many improvements to be a reality in scale-up.

**Acknowledgments**

The authors acknowledge Dr. Gian Luca Chiarello, Department of Chemistry, University of Milano, for the measurement of the emission spectrum of the lamp.

**References**

Andronic, L., Isac, L., Miralles-Cuevas, S., Visa, M., Oller, I., Duta, A. and Malato, S. (2016) Pilot-plant evaluation of TiO2 and TiO2-based hybrid photocatalysts for solar treatment of polluted water. Journal of Hazardous materials 320, 469-478.

Balest, L., Mascolo, G., Di Iaconi, C. and Lopez, A. (2008) Removal of endocrine disrupter compounds from municipal wastewater by an innovative biological technology. Water Science and Technology 58(4), 953-956.

503 Bayati, M.R., Moshfegh, A.Z. and Golestani-Fard, F. (2010) In situ growth of vanadia–titania
504 nano/micro-porous layers with enhanced photocatalytic performance by micro-arc oxidation.
505 Electrochimica Acta 55(9), 3093-3102.
506 Bestetti, M., Franz, S., Cuzzolin, M., Arosio, P. and Cavallotti, P.L. (2007) Structure of
507 nanotubular titanium oxide templates prepared by electrochemical anodization in H2SO4/HF
508 solutions. Thin Solid Films 515(13), 5253-5258.
509 Borges, M., García, D., Hernández, T., Ruiz-Morales, J. and Esparza, P. (2015) Supported
510 Photocatalyst for Removal of Emerging Contaminants from Wastewater in a Continuous
511 Packed-Bed Photoreactor Configuration. Catalysts 5(1), 77.
512 Byrne, C., Subramanian, G. and Pillai, S. (2017) Recent Advances in Photocatalysis for
513 Environmental Applications.
514 Castiglioni, S., Davoli, E., Riva, F., Palmiotto, M., Camporini, P., Manenti, A. and Zuccato, E.
515 (2018) Mass balance of emerging contaminants in the water cycle of a highly urbanized and
516 industrialized area of Italy. Water Research 131, 287-298.
517 Cates, E.L. (2017) Photocatalytic Water Treatment: So Where Are We Going with This?
518 Environmental Science & Technology 51(2), 757-758.
519 Comparelli, R., Cozzoli, P.D., Curri, M.L., Agostiano, A., Mascolo, G. and Lovecchio, G. (2004)
520 Photocatalytic degradation of methyl-red by immobilised nanoparticles of TiO2 and ZnO. Water
521 Science & Technology 49(4), 183-188.
522 Del Moro, G., Mancini, A., Mascolo, G. and Di Iaconi, C. (2013) Comparison of UV/H2O2 based
523 AOP as an end treatment or integrated with biological degradation for treating landfill
524 leachates. Chemical Engineering Journal 218, 133-137.

525 Del Moro, G., Prieto-Rodríguez, L., De Sanctis, M., Di Iaconi, C., Malato, S. and Mascolo, G.
526 (2016) Landfill leachate treatment: Comparison of standalone electrochemical degradation and
527 combined with a novel biofilter. Chemical Engineering Journal 288, 87-98.
528 Detomaso, A., Mascolo, G. and Lopez, A. (2005) Characterization of carbofuran
529 photodegradation by-products by liquid chromatography/hybrid quadrupole time-of-flight
530 mass spectrometry. Rapid Communications in Mass Spectrometry 19(15), 2193-2202.
531 Dong, H., Zeng, G., Tang, L., Fan, C., Zhang, C., He, X. and He, Y. (2015) An overview on
532 limitations of TiO2-based particles for photocatalytic degradation of organic pollutants and the
533 corresponding countermeasures. Water Research 79, 128-146.
534 Fagan, R., McCormack, D.E., Dionysiou, D.D. and Pillai, S.C. (2016) A review of solar and visible
535 light active TiO2 photocatalysis for treating bacteria, cyanotoxins and contaminants of
536 emerging concern. Materials Science in Semiconductor Processing 42, 2-14.
537 Franz, S., Perego, D., Marchese, O. and Bestetti, M. (2015) Photoelectrochemical advanced
538 oxidation processes on nanostructured TiO2 catalysts: Decolorization of a textile azo-dye.
539 Journal of Water Chemistry and Technology 37(3), 108-115.
540 Franz, S., Perego, D., Marchese, O., Lucotti, A. and Bestetti, M. (2016) Photoactive TiO2 coatings
541 obtained by Plasma Electrolytic Oxidation in refrigerated electrolytes. Applied Surface Science
542 385, 498-505.
543 Giannakis, S., Gamarra Vives, F.A., Grandjean, D., Magnet, A., De Alencastro, L.F. and Pulgarin,
544 C. (2015) Effect of advanced oxidation processes on the micropollutants and the effluent
545 organic matter contained in municipal wastewater previously treated by three different
546 secondary methods. Water Research 84, 295-306.

547 Guijas, C., Montenegro-Burke, J.R., Domingo-Almenara, X., Palermo, A., Warth, B., Hermann, G.,
548 Koellensperger, G., Huan, T., Uritboonthai, W., Aisporna, A.E., Wolan, D.W., Spilker, M.E.,
549 Benton, H.P. and Siuzdak, G. (2018) METLIN: A Technology Platform for Identifying Knowns and
550 Unknowns. Analytical Chemistry 90(5), 3156-3164.
551 Joss, A., Keller, E., Alder, A.C., Göbel, A., McArdell, C.S., Ternes, T. and Siegrist, H. (2005)
552 Removal of pharmaceuticals and fragrances in biological wastewater treatment. Water
553 Research 39(14), 3139-3152.
554 Kasprzyk-Hordern, B., Dinsdale, R.M. and Guwy, A.J. (2009) The removal of pharmaceuticals,
555 personal care products, endocrine disruptors and illicit drugs during wastewater treatment and
556 its impact on the quality of receiving waters. Water Research 43(2), 363-380.
557 Liu, F., Song, Y., Wang, F., Shimizu, T., Igarashi, K. and Zhao, L. (2005) Formation
558 characterization of hydroxyapatite on titanium by microarc oxidation and hydrothermal
559 treatment. Journal of bioscience and bioengineering 100(1), 100-104.
560 Logar, I., Brouwer, R., Maurer, M. and Ort, C. (2014) Cost-Benefit Analysis of the Swiss National
561 Policy on Reducing Micropollutants in Treated Wastewater. Environmental Science &
562 Technology 48(21), 12500-12508.
563 Loos, M. (2018) EnviMass version 3.5 LC-HRMS trend detection workflow - R package.
564 Loos, R., Carvalho, R., António, D.C., Comero, S., Locoro, G., Tavazzi, S., Paracchini, B., Ghiani,
565 M., Lettieri, T., Blaha, L., Jarosova, B., Voorspoels, S., Servaes, K., Haglund, P., Fick, J., Lindberg,
566 R.H., Schwesig, D. and Gawlik, B.M. (2013) EU-wide monitoring survey on emerging polar
567 organic contaminants in wastewater treatment plant effluents. Water Research 47(17), 6475-
568 6487.

569 Luo, Y., Guo, W., Ngo, H.H., Nghiem, L.D., Hai, F.I., Zhang, J., Liang, S. and Wang, X.C. (2014) A
570 review on the occurrence of micropollutants in the aquatic environment and their fate and
571 removal during wastewater treatment. Science of The Total Environment 473-474, 619-641.
572 Mascolo, G., Lopez, A., Detomaso, A. and Lovecchio, G. (2005) Ion chromatography-
573 electrospray mass spectrometry for the identification of low-molecular-weight organic acids
574 during the 2,4-dichlorophenol degradation. Journal of Chromatography A 1067(1-2), 191-196.
575 Miklos, D.B., Remy, C., Jekel, M., Linden, K.G., Drewes, J.E. and Hübner, U. (2018) Evaluation of
576 advanced oxidation processes for water and wastewater treatment – A critical review. Water
577 Research 139, 118-131.
578 Mirelman, L.K., Curran, J.A. and Clyne, T.W. (2012) The production of anatase-rich photoactive
579 coatings by plasma electrolytic oxidation. Surface and Coatings Technology 207, 66-71.
580 Murgolo, S., Yargeau, V., Gerbasi, R., Visentin, F., El Habra, N., Ricco, G., Lacchetti, I., Carere, M.,
581 Curri, M.L. and Mascolo, G. (2017) A new supported TiO2 film deposited on stainless steel for
582 the photocatalytic degradation of contaminants of emerging concern. Chemical Engineering
583 Journal 318, 103-111.
584 Nakata, K. and Fujishima, A. (2012) TiO2 photocatalysis: Design and applications. Journal of
585 Photochemistry and Photobiology C: Photochemistry Reviews 13(3), 169-189.
586 Nie, X., Leyland, A. and Matthews, A. (2000) Deposition of layered bioceramic
587 hydroxyapatite/TiO2 coatings on titanium alloys using a hybrid technique of micro-arc oxidation
588 and electrophoresis. Surface and Coatings Technology 125(1), 407-414.

589 Ochiai, T. and Fujishima, A. (2012) Photoelectrochemical properties of TiO2 photocatalyst and
590 its applications for environmental purification. Journal of Photochemistry and Photobiology C:
591 Photochemistry Reviews 13(4), 247-262.
592 Pagano, M., Lopez, A., Volpe, A., Mascolo, G. and Ciannarella, R. (2008) Oxidation of nonionic
593 surfactants by Fenton and H2O2/UV processes. Environmental Technology 29(4), 423-433.
594 Petronella, F., Diomede, S., Fanizza, E., Mascolo, G., Sibillano, T., Agostiano, A., Curri, M.L. and
595 Comparelli, R. (2013) Photodegradation of nalidixic acid assisted by TiO2 nanorods/Ag
596 nanoparticles based catalyst. Chemosphere 91(7), 941-947.
597 Petronella, F., Fanizza, E., Mascolo, G., Locaputo, V., Bertinetti, L., Martra, G., Coluccia, S.,
598 Agostiano, A., Curri, M.L. and Comparelli, R. (2011) Photocatalytic Activity of Nanocomposite
599 Catalyst Films Based on Nanocrystalline Metal/Semiconductors. Journal of Physical Chemistry C
600 115(24), 12033-12040.
601 Rice, E., Baird, R., Eaton, A. and Clesceri, L. (2012) Standard Methods for the Examination of
602 Water and Wastewater.
603 Rizzo, L., Malato, S., Antakyali, D., Beretsou, V.G., Đolić, M.B., Gernjak, W., Heath, E., Ivancev-
604 Tumbas, I., Karaolia, P., Lado Ribeiro, A.R., Mascolo, G., McArdell, C.S., Schaar, H., Silva, A.M.T.
605 and Fatta-Kassinos, D. (2019) Consolidated vs new advanced treatment methods for the
606 removal of contaminants of emerging concern from urban wastewater. Science of The Total
607 Environment 655, 986-1008.
608 Schollée, J.E., Bourgin, M., von Gunten, U., McArdell, C.S. and Hollender, J. (2018) Non-target
609 screening to trace ozonation transformation products in a wastewater treatment train including
610 different post-treatments. Water Research 142, 267-278.

611 Schröder, P., Helmreich, B., Škrbić, B., Carballa, M., Papa, M., Pastore, C., Emre, Z., Oehmen, A.,
612 Langenhoff, A., Molinos, M., Dvarioniene, J., Huber, C., Tsagarakis, K.P., Martinez-Lopez, E.,
613 Pagano, S.M., Vogelsang, C. and Mascolo, G. (2016) Status of hormones and painkillers in
614 wastewater effluents across several European states—considerations for the EU watch list
615 concerning estradiols and diclofenac. Environmental Science and Pollution Research 23(13),
616 12835-12866.
617 Schymanski, E.L., Jeon, J., Gulde, R., Fenner, K., Ruff, M., Singer, H.P. and Hollender, J. (2014)
618 Identifying Small Molecules via High Resolution Mass Spectrometry: Communicating
619 Confidence. Environmental Science & Technology 48(4), 2097-2098.
620 Sousa, J.C.G., Ribeiro, A.R., Barbosa, M.O., Pereira, M.F.R. and Silva, A.M.T. (2018) A review on
621 environmental monitoring of water organic pollutants identified by EU guidelines. Journal of
622 Hazardous Materials 344, 146-162.
623 Spurr, R.A. and Myers, H. (1957) Quantitative Analysis of Anatase-Rutile Mixtures with an X-Ray
624 Diffractometer. Analytical Chemistry 29(5), 760-762.
625 Stalter, D., Magdeburg, A., Weil, M., Knacker, T. and Oehlmann, J. (2010) Toxication or
626 detoxication? In vivo toxicity assessment of ozonation as advanced wastewater treatment with
627 the rainbow trout. Water Research 44(2), 439-448.
628 Ternes, T.A. (1998) Occurrence of drugs in German sewage treatment plants and
629 rivers1Dedicated to Professor Dr. Klaus Haberer on the occasion of his 70th birthday.1. Water
630 Research 32(11), 3245-3260.

631 Tran, N.H., Reinhard, M. and Gin, K.Y.-H. (2018) Occurrence and fate of emerging contaminants
632 in municipal wastewater treatment plants from different geographical regions-a review. Water
633 Research 133, 182-207.
634 Trasatti, S. and Petrii, O.A. (1991) Real surface area measurements in electrochemistry, p. 711.
635 Wei, D., Zhou, Y., Jia, D. and Wang, Y. (2008) Chemical treatment of TiO2-based coatings
636 formed by plasma electrolytic oxidation in electrolyte containing nano-HA, calcium salts and
637 phosphates for biomedical applications. Applied Surface Science 254(6), 1775-1782.
638 Yerokhin, A.L., Nie, X., Leyland, A., Matthews, A. and Dowey, S.J. (1999) Plasma electrolysis for
639 surface engineering. Surface and Coatings Technology 122(2), 73-93.
640 Zhou, J.L., Zhang, Z.L., Banks, E., Grover, D. and Jiang, J.Q. (2009) Pharmaceutical residues in
641 wastewater treatment works effluents and their impact on receiving river water. Journal of
642 Hazardous materials 166(2), 655-661.
643 Zwiener, C., Seeger, S., Glauner, T. and Frimmel, F. (2002) Metabolites from the biodegradation
644 of pharmaceutical residues of ibuprofen in biofilm reactors and batch experiments. Analytical
645 and Bioanalytical Chemistry 372(4), 569-575.

646

647 **Table 1**

648

649

650 Table 1. Characteristics of the employed real secondary wastewater effluent.

651

| parameter | range value (min-max) |
|---|---|
| Flow rate | 432,000 $m^3$ $d^{-1}$ |
| Population equivalent | 1,250,000 |
| pH | 7.3÷8 |
| conductivity | 720÷950 µS $cm^{-1}$ |
| COD | 30÷60 mg $L^{-1}$ |
| $BOD_5$ | < 15 mg $L^{-1}$ |
| TOC | 12÷25 mg $L^{-1}$ |
| DOC | 10÷22 mg $L^{-1}$ |
| $Cl^-$ | 200÷260 mg $L^{-1}$ |
| $N\text{-}NO_3$ | 2÷4 mg $L^{-1}$ |
| $N\text{-}NH_4$ | < 5 mg $L^{-1}$ |
| Total N | < 10 mg $L^{-1}$ |
| Total P | 0.9÷1.5 mg $L^{-1}$ |
| SST | < 15 mg $L^{-1}$ |

652

653

654 **Table 2**

655

656 Table 2. List of transformation reactions considered for linkage analysis with the indication of
657 the exact mass difference and formula difference between the parent compound and
658 transformation product as a result of the transformation reaction.

659

| Transformation reaction | Formula difference | Exact m/z difference |
|---|---|---|
| Glucuronidation | $+C_6H_8O_6$ | 176.032 |
| Sulfation | $+SO_3$ | 79.9568 |
| Addition of 3 atoms of oxygen | +3O | 47.9847 |
| Acetylation | $+C_2H_2O$ | 42.0106 |
| Addition of 2 atoms of oxygen | +2O | 31.9898 |
| Methyl to carboxylic acid, amine to nitro | -2H+2O | 29.9741 |
| Hydration | $+H_2O$ | 18.0106 |
| Hydroxylation, N or S-oxidation, epoxidation | +O | 15.9949 |
| Oxidative deamination | $-NH_3$+2O | 14.9632 |
| Alcohol to carboxylic acid or primary amine to nitro | -2H+O | 13.9792 |
| Oxidative displacement of amine | -NH +OH | 1.9918 |
| Deamination to ketone | $-NH_3$+O | -1.0317 |
| Demethylation | $-CH_2$ | -14.0157 |
| Dehydration | $-H_2O$ | -18.0106 |
| Di-demethyl or de-ethylation | $-C_2H_4$ | -28.0313 |
| Dealkylation | $-C_2H_6$ | -30.047 |
| De-acetylation | $-C_2H_2O$ | -42.0106 |
| Decarboxylation | $-CO_2$ | -43.9898 |
| Loss of nitro group | $-NO_2$+H | -44.9851 |
| De-sulfation | $-SO_3$ | -79.9568 |
| De-glucuronidation | $-C_6H_8O_6$ | -176.032 |

660

661

662 **Figure Captions**

663

664 Figure 1. SEM micrographs, surface and cross-section (inset), of the $TiO_2$ film (a), GDOES in-
665 depth profile of Titanium and Oxygen elements into the TiO2 film (b), XRD pattern of
666 the $TiO_2$ films (A=Anatase; R=Rutile; T=Titanium substrate) (c) and IPCE of $TiO_2$ films
667 obtained by PEO as a function of the applied voltage (d).

668 Figure 2. Degradation of carbamazepine by photoelectrocatalysis and conventional
669 photocatalysis (Degussa P25) performed in real secondary effluent wastewater. Error
670 bars represent the standard deviation obtained for three replicates.

671 Figure 3. Replicates of carbamazepine degradation in real secondary effluent wastewater by
672 photoelectrocatalysis (a) and aging effect of the nanostructured $TiO_2$ meshes along
673 prolonged use and recovery of the initial performance by re-anodization (b).

674 Figure 4. Box-whisker plots of kinetic constants for the 51 suspect CECs identified by the
675 analytical screening procedure (Table S1) during degradation by photolysis,
676 photocatalysis with supported $TiO_2$ and electrochemical photocatalysis
677 ($TiO_2$+Bias+UV) in real secondary effluent wastewater. Boxplots represent the
678 distance between the first and third quartiles while whiskers are set as the most
679 extreme (lower and upper) data point not exceeding 1.5 times the quartile range
680 from the median. Kinetic constants outside such a range are outliers.

681 Figure 5. Box-whisker plots of peak area for the 194 TPs (a) and for all 395 compounds (194
682 TPs + 201 compounds present in the secondary wastewater effluent) detected by the

683 analytical screening procedure (Table S2) during degradation by photolysis,
684 photocatalysis with supported $TiO_2$ and electrochemical photocatalysis
685 ($TiO_2$+Bias+UV) in real secondary effluent wastewater at 45 and 90 min reaction time.
686 Boxplots represent the distance between the first and third quartiles while whiskers
687 are set as the most extreme (lower and upper) data point not exceeding 1.5 times the
688 quartile range from the median. Values outside such a range are outliers.

689 Figure 6. Radar plot of the different transformation reactions detected by linkage analysis
690 considering as parent compounds all the 201 compounds listed in Table S1 (blue line)
691 or the 51 suspect CECs detected within such a list (red line). The scale, indicated on
692 the grey concentric circles, shows the number of times each transformation reaction
693 was detected.

694 Figure 7. Proposed degradation pathway of carbamazepine obtained on the basis of the
695 transformation reactions detected by the linkage analysis. TPs are named with their
696 nominal mass.

697 Figure 8. Proposed degradation pathway of 1-piperidinoacetone obtained on the basis of the
698 transformation reactions detected by the linkage analysis. The two other possible
699 chemical structures, namely tropine and azonan-2-one, are also shown.

700

701 **Figure 1**

702

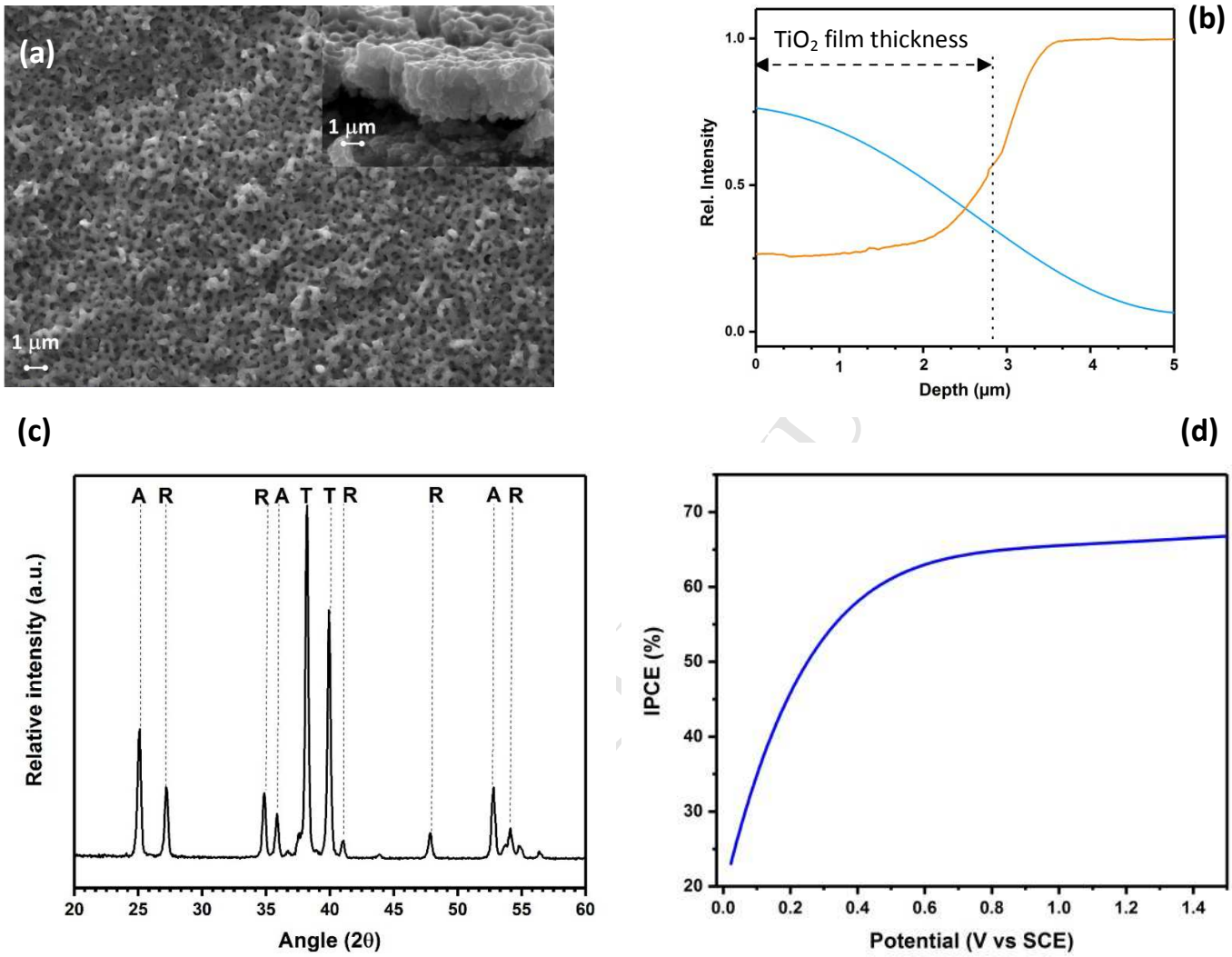


703

704 Figure 1. SEM micrographs, surface and cross-section (inset), of the $TiO_2$ film (a), GDOES in-
705 depth profile of Titanium and Oxygen elements into the TiO2 film (b), XRD pattern of
706 the $TiO_2$ films (A=Anatase; R=Rutile; T=Titanium substrate) (c) and IPCE of $TiO_2$ films
707 obtained by PEO as a function of the applied voltage (d).

708

709 **Figure 2**

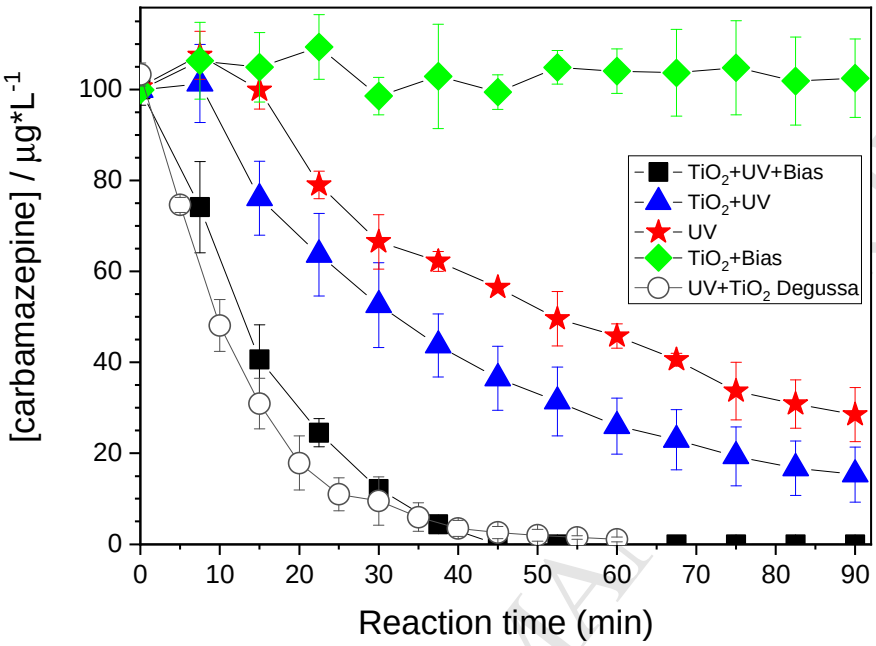


710

711

712 Figure 2. Degradation of carbamazepine by photoelectrocatalysis and conventional

713 photocatalysis (Degussa P25) performed in real secondary effluent wastewater.

714 Error bars represent the standard deviation obtained for three replicates.

715 **Figure 3**

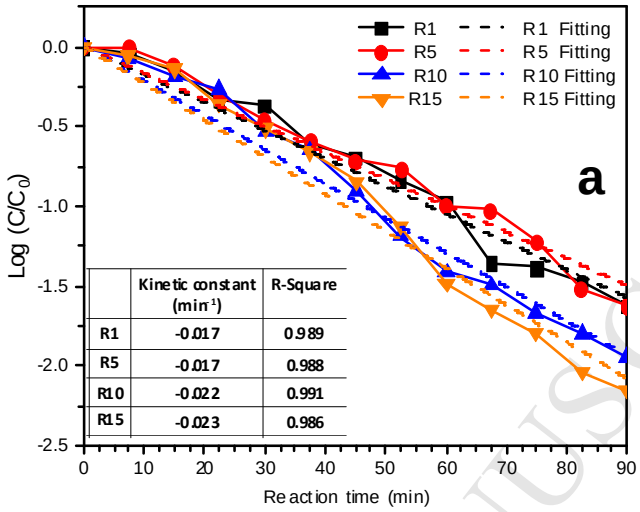


716

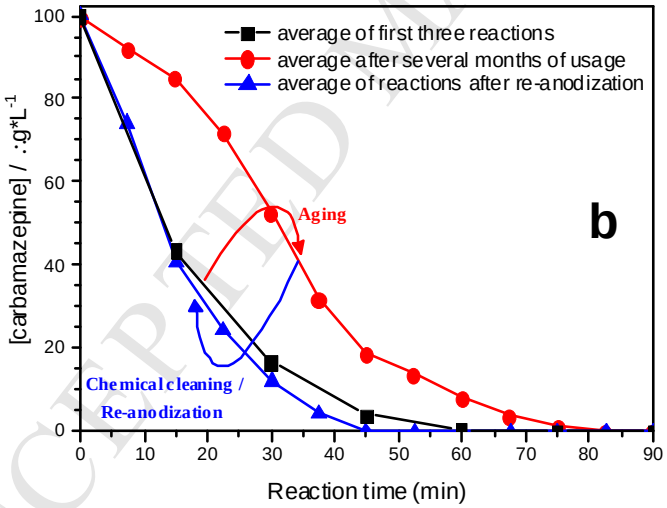


717

718 Figure 3. Replicates of carbamazepine degradation in real secondary effluent wastewater by

719 photoelectrocatalysis (a) and aging effect of the nanostructured $TiO_2$ meshes along

720 prolonged use and recovery of the initial performance by re-anodization (b).

721 **Figure 4**

722

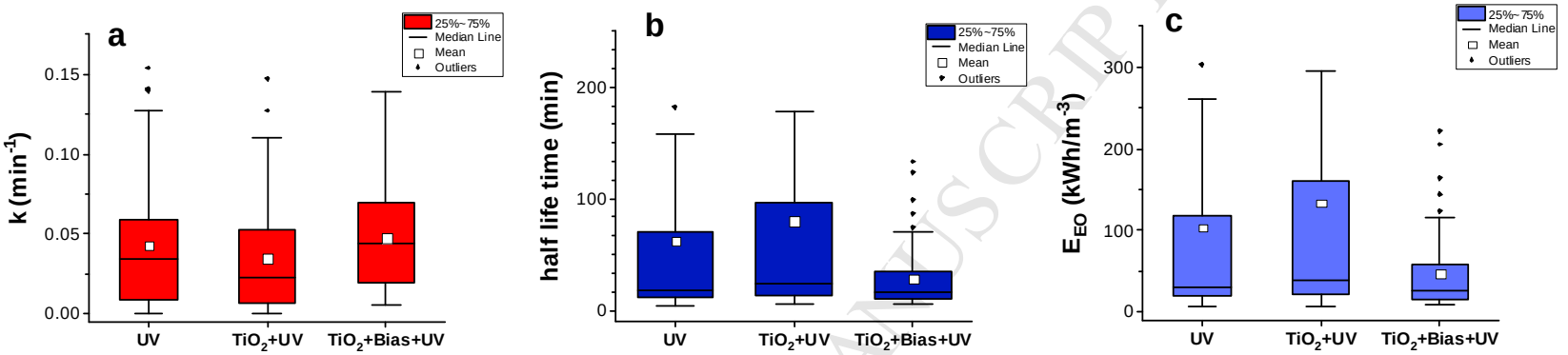


723

724

725 Figure 3. Box-whisker plots of (a) kinetic constants, (b) half-life times and (c) Electrical Energy per Order of magnitude of removal

726 ($E_{EO}$) for the 51 suspect CECs identified by the analytical screening procedure (Table S1) during degradation by photolysis,

727 photocatalysis with supported $TiO_2$ and electrochemical photocatalysis ($TiO_2$+Bias+UV) in real secondary effluent

728 wastewater. Boxplots represent the distance between the first and third quartiles while whiskers are set as the most

729 extreme (lower and upper) data point not exceeding 1.5 times the quartile range from the median. Kinetic constants

730 outside such a range are outliers.

731 **Figure 5**

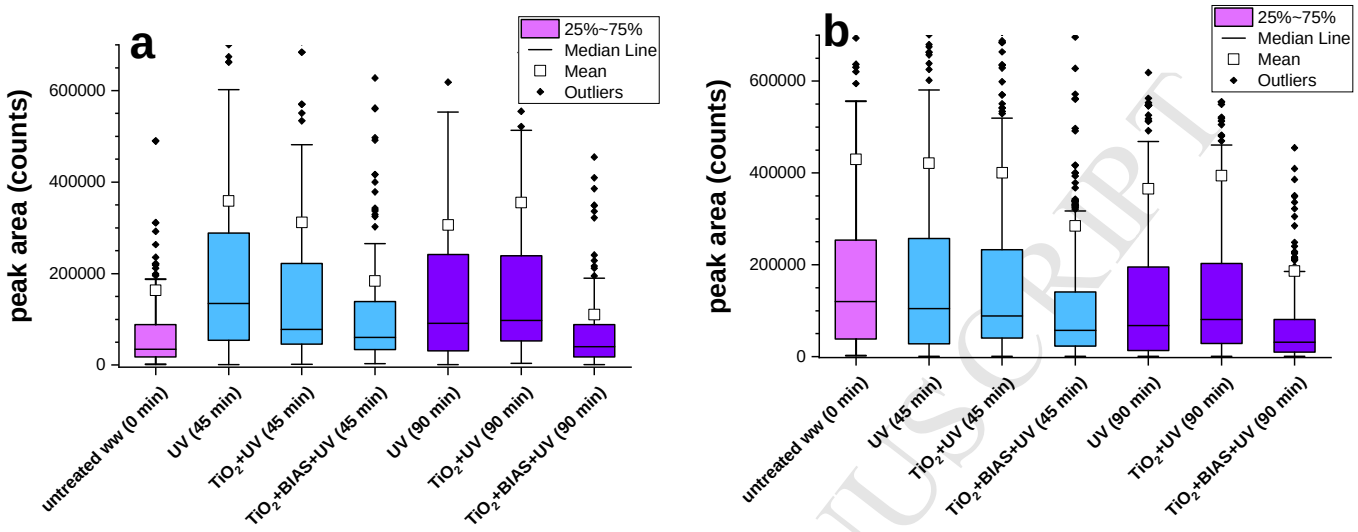


732

733

734 Figure 4. Box-whisker plots of peak area for the 194 TPs (a) and for all 395 compounds (194
735 TPs + 201 compounds present in the secondary wastewater effluent) detected by the
736 analytical screening procedure (Table S2) during degradation by photolysis,
737 photocatalysis with supported $TiO_2$ and electrochemical photocatalysis
738 ($TiO_2$+Bias+UV) in real secondary effluent wastewater at 45 and 90 min reaction time.
739 Boxplots represent the distance between the first and third quartiles while whiskers
740 are set as the most extreme (lower and upper) data point not exceeding 1.5 times the
741 quartile range from the median. Values outside such a range are outliers.

742

743 **Figure 6**

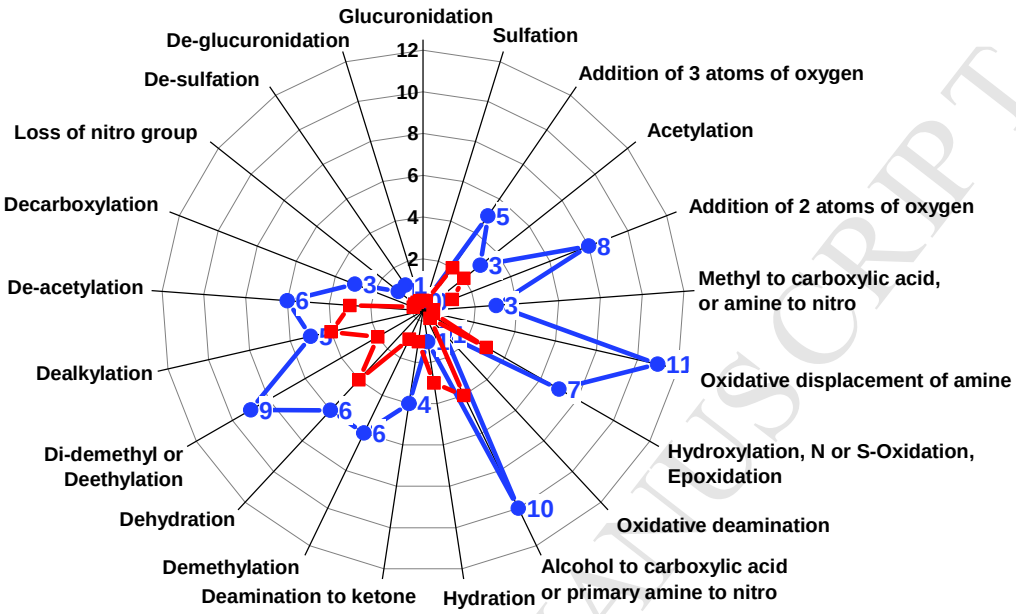


744

745 Figure 5. Radar plot of the different transformation reactions detected by linkage analysis
746 considering as parent compounds all the 201 compounds listed in Table S1 (blue line)
747 or the 51 suspect CECs detected within such a list (red line). The scale, indicated on
748 the grey concentric circles, shows the number of times each transformation reaction
749 was detected.

750

751 **Figure 7**

752

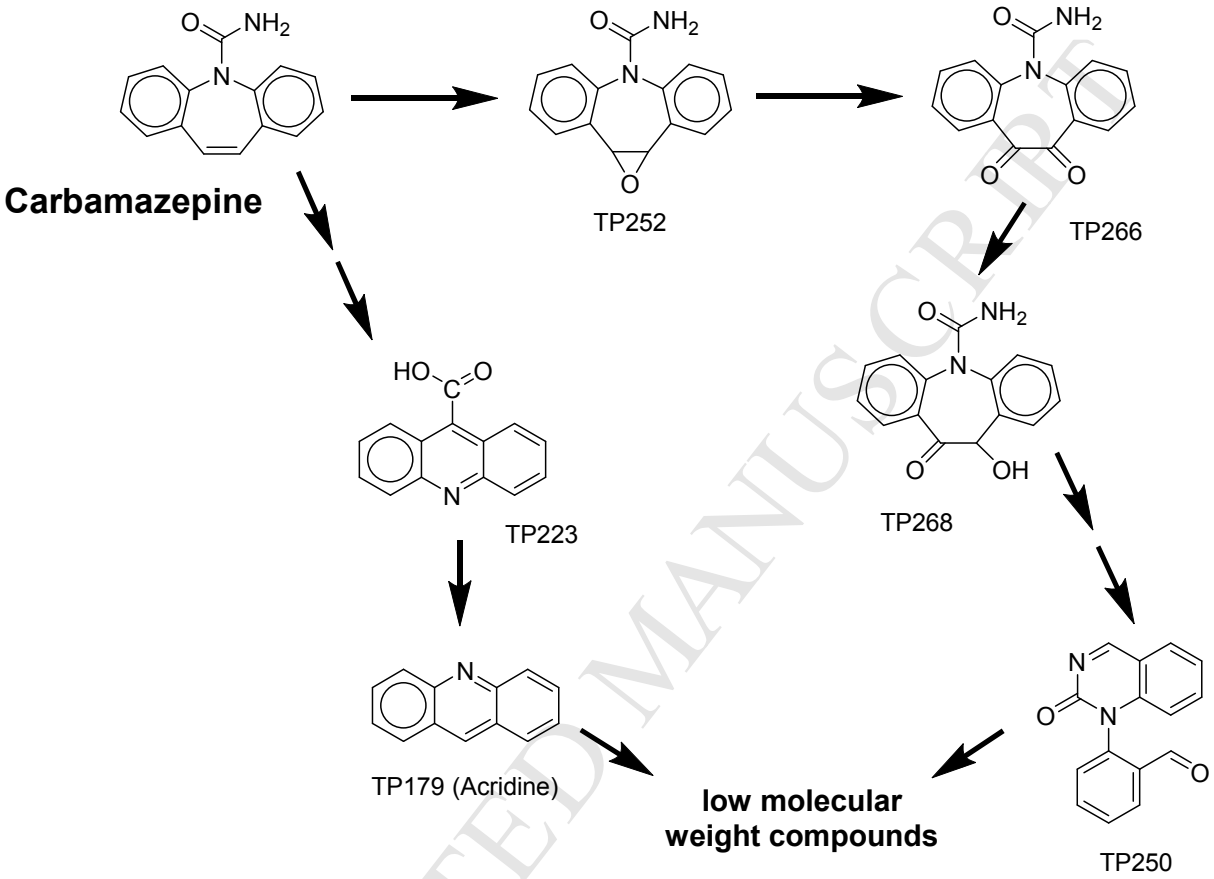


753

754

755 Figure 6. Proposed degradation pathway of carbamazepine obtained on the basis of the
756 transformation reactions detected by the linkage analysis. TPs are named with their
757 nominal mass.

758

759 **Figure 8**

760

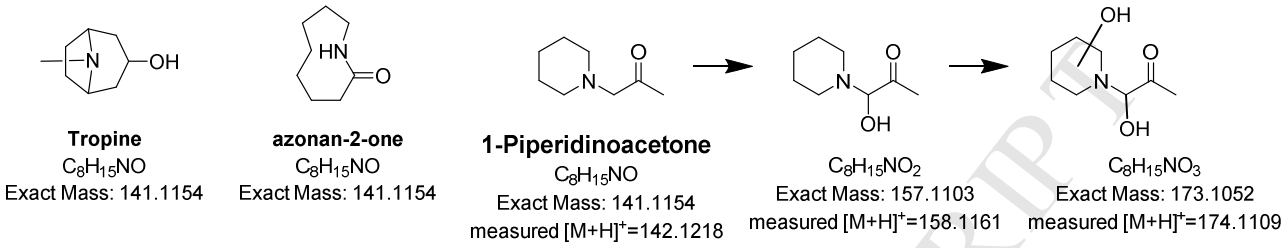


761
762

763

764 Figure 7. Proposed degradation pathway of 1-piperidinoacetone obtained on the basis of the
765 transformation reactions detected by the linkage analysis. The two other possible
766 chemical structures, namely tropine and azonan-2-one, are also shown.

**HIGHLIGHTS**

- immobilized $TiO_2$ on titanium mesh was used for CECs photocatalysis in wastewater
- over 200 organic compounds present in secondary wastewater effluent were removed
- The supported catalyst was positively tested for 15 cycles
- The electrophotocatalityc process can be used for removing CECs in real wastewater